J|A|C|S
ARTICLES
Published on Web 06/07/2007

Barriers to Ion Translocation in Cationic and Anionic Receptors from the Cys-Loop Family

Ivaylo Ivanov,*[,†,‡,⊥] Xiaolin Cheng,[†,§,⊥] Steven M. Sine,[#] and J. Andrew McCammon[†,‡,§,⊥]

Contribution from the Department of Chemistry and Biochemistry, Department of Pharmacology, Howard Hughes Medical Institute, and Center for Theoretical Biological Physics, University of California—San Diego, 9500 Gilman Drive, La Jolla, California 92093-0365, and Department of Physiology and Biomedical Engineering, Mayo Clinic College of Medicine, Rochester, Minnesota 55905

Received February 7, 2007; E-mail: iivanov@mccammon.ucsd.edu

Abstract: Understanding the mechanisms of gating and ion permeation in biological channels and receptors has been a long-standing challenge in biophysics. Recent advances in structural biology have revealed the architecture of a number of transmembrane channels and allowed detailed, molecular-level insight into these systems. Herein, we have examined the barriers to ion conductance and origins of ion selectivity in models of the cationic human α7 nicotinic acetylcholine receptor (nAChR) and the anionic α1 glycine receptor (GlyR), based on the structure of *Torpedo* nAChR. Molecular dynamics simulations were used to determine water density profiles along the channel length, and they established that both receptor pores were fully hydrated. The very low water density in the middle of the nAChR pore indicated the existence of a hydrophobic constriction. By contrast, the pore of GlyR was lined with hydrophilic residues and remained well-hydrated throughout. Adaptive biasing force simulations allowed us to reconstruct potentials of mean force (PMFs) for chloride and sodium ions in the two receptors. For the nicotinic receptor we observed barriers to ion translocation associated with rings of hydrophobic residues—Val13′ and Leu9′—in the middle of the transmembrane domain. This finding further substantiates the hydrophobic gating hypothesis for nAChR. The PMF revealed no significant hydrophobic barrier for chloride translocation in GlyR. For both receptors nonpermeant ions displayed considerable barriers. Thus, the overall electrostatics and the presence of rings of charged residues at the entrance and exit of the channels were sufficient to explain the experimentally observed anion and cation selectivity.

Introduction

The nicotinic acetylcholine (nAChR) and glycine (GlyR) receptors belong to the Cys-loop family of receptors[1,2] and select for either cations or anions, respectively. Together these two classes of receptors mediate the majority of fast synaptic transmission throughout the nervous system. Their major function is to bind the neurotransmitter and change the membrane potential through selective permeation of ions. The nAChR is excitatory and conducts Na^+ and K^+ ions, and in some subunit combinations, Ca^{2+} ions. The GlyR, on the other hand, is inhibitory and conducts Cl^- ions.

Progress toward understanding the function of Cys-loop receptors was, until recently, hindered by the absence of detailed structural data. A recent cryoelectron microscopy (cryo-EM) structure of nAChR from *Torpedo marmorata*[3] has, in part, reversed this situation and revealed the overall architecture of this ion channel, comprising extracellular (EC), transmembrane (TM), and intracellular (IC) domains (Figure 1). Binding of neurotransmitters to the EC domain is thought to alter the dynamic equilibrium between the open and closed states of the channel. How the conformational change upon binding propagates over an approximately 40 Å distance to the TM domain is, however, unknown.

The cryo-EM structure identified a possible hydrophobic obstruction in the channel pore comprising residues Val 13′, Leu 9′ in the pore-lining M2 helices (Figure 2) that in the closed state may form the barrier to ion flow. Nevertheless, the exact location of the constriction point has not been definitively ascertained, and different experimental approaches have led to conflicting proposed locations: (i) residues at positions 9′ and 13′ of M2 that form a hydrophobic girdle,[4,5] (ii) residues at positions 2′ through 6′ near the intracellular end of M2,[1,6,7] or (iii) a location closer to the extracellular entrance of the channel.[8,9]

† Department of Chemistry and Biochemistry, University of California—San Diego.
‡ Department of Pharmacology, University of California—San Diego.
§ Howard Hughes Medical Institute, University of California—San Diego.
⊥ Center for Theoretical Biological Physics, University of California—San Diego.
Mayo Clinic College of Medicine.

(1) Karlin, A. *Nat. Rev. Neurosci.* **2002**, *3*, 102−114.
(2) Sine, S. M.; Engel, A. G. *Nature* **2006**, *440*, 448−455.
(3) Unwin, N. *J. Mol. Biol.* **2005**, *346*, 967−989.
(4) Miyazawa, A.; Fujiyoshi, Y.; Unwin, N. *Nature* **2003**, *423*, 949−955.
(5) Panicker, S.; Cruz, H.; Arrabit, C.; Slesinger, P. A. *J. Neurosci.* **2002**, *22*, 1629−1639.
(6) Wilson, G. G.; Karlin, A. *Neuron* **1998**, *20*, 1269−1281.

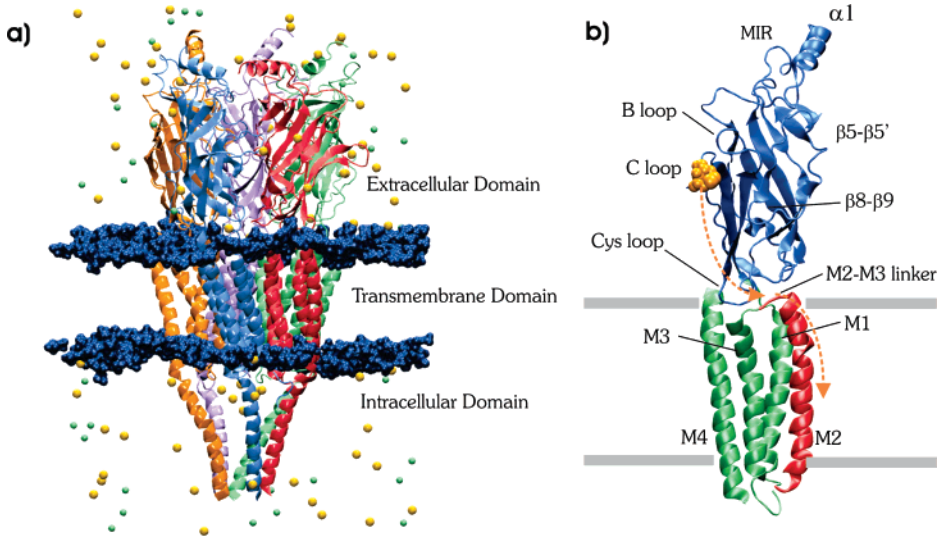

Figure 1. (a) Structure of α7 nAChR with the five subunits highlighted in different colors; chloride ions are shown in green, sodium ions are in yellow, the head group region of the lipid bilayer is in dark blue. (b) Structure of a single subunit of nAChR (for clarity only the extracellular (blue) and transmembrane domains (green) are shown); the pore-lining M2 helix is highlighted in red; the yellow arrows indicate the direction of the motion along the putative allosteric pathway from the tip of the C-loop (close to the ligand-binding site) to the hydrophobic gate at the center of the M2 helix. The present simulations were carried out for the transmembrane domain of the nAChR and GlyR receptors.

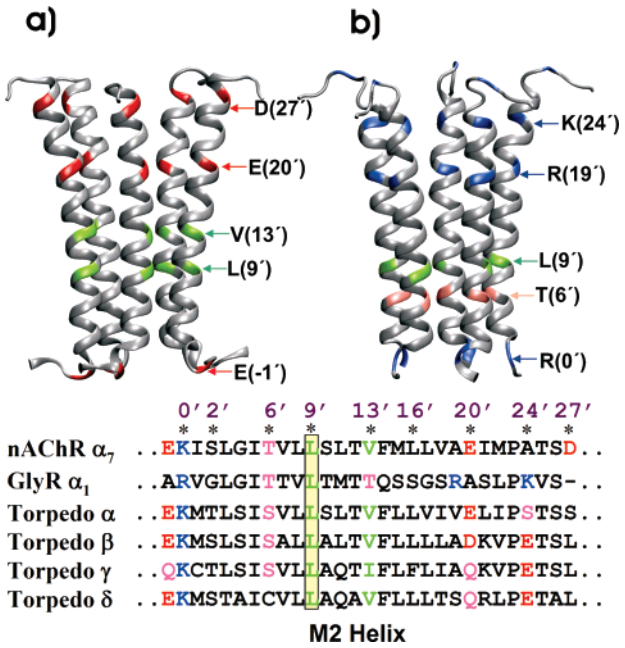

Figure 2. Homology models of the M2 helix bundle of (a) the human α7 nAChR and (b) the α1 GlyR. The sequence alignment of the M2 residues of α7 nAChR, α1 GlyR, and nAChR from *T. marmorata*.

Thus, despite the vital biological role of Cys-loop receptors and considerable experimental and theoretical effort devoted to their study, many outstanding questions regarding their structural characteristics and function remain unanswered: how does the binding of neurotransmitter initiate allosteric control over the TM domain; what is the nature of the gating mechanism and the location of the gate; what is the origin of cation versus anion selectivity among members of the Cys-loop receptor superfamily? To begin to address these issues we calculated effective free energy profiles for sodium and chloride ions along the lengths of the TM pores of these two classes of receptors.

Results and Discussion

First, we investigated the hydration of the channel pore of the homopentameric human α7 nAChR and α1 GlyR. Although the cryo-EM structure of the *Torpedo* nAChR was obtained without a ligand,[3] and thus is supposed to represent a closed state of the channel, it showed that the pore formed by the set of five transmembrane M2 helices was not fully occluded. At the narrowest point, the pore radius (~2.5 Å) is large enough to accommodate water molecules and, perhaps, partially desolvated ions (Supporting Information Figure S1). However, besides purely geometric factors such as the radius, dynamic and electrostatic factors have been shown to play a crucial role in determining hydration in narrow pores and nanotubes.[10] Recent simulation studies reached different conclusions regarding pore hydration. Simulations by Corry[11] and Hung et al.[12] of the full TM domain of *Torpedo* nAChR found the pore was water-filled throughout its length, whereas a study by Saiz and Klein of an assembly of five M2 helices found water was excluded by a hydrophobic obstruction in the middle of the pore after only 4−5 ns of molecular dynamics simulation.[13] Variations in the size of the models, differences in the simulation protocols (e.g., the application of restraints), or the force field parameters may have contributed to these divergent outcomes. To clarify this issue, it is worth examining larger models, comprising the entire TM domain of α7 nAChR and α1 GlyR, along with judicious use of restraints only at the M1−M2 and M2−M3 linkers at the opposite ends of the channel. Thus, our simulations address two questions relevant to ion permeation. First, is the receptor pore fully hydrated or is water excluded from the TM domain as proposed in the vapor-lock mechanism

(7) Paas, Y.; Gibor, G.; Grailhe, R.; Savatier-Duclert, N.; Dufresne, V.; Sunesen, M.; de Carvalho, L. P.; Changeux, J. P.; Attali, B. *Proc. Natl. Acad. Sci. U.S.A.* **2005**, *102*, 15877−15882.
(8) England, P. M.; Zhang, Y.; Dougherty, D. A.; Lester, H. A. *Cell* **1999**, *96*, 89−98.
(9) Labarca, C.; Nowak, M. W.; Zhang, H.; Tang, L.; Deshpande, P.; Lester, H. A. *Nature* **1995**, *376*, 514−516.
(10) Hummer, G.; Rasaiah, J. C.; Noworyta, J. P. *Nature* **2001**, *414*, 188−190.
(11) Corry, B. *Biophys. J.* **2006**, *90*, 799−810.
(12) Hung, A.; Tai, K.; Sansom, M. S. *Biophys. J.* **2005**, *88*, 3321−3333.
(13) Saiz, L.; Klein, M. L. *Biophys. J.* **2005**, *88*, 959−970.

for the MscS channel?[14] Second, if the pore is fully hydrated, can it hinder the passage of solvated ions, even though it may not prevent individual water molecules from going through?

To address the first question we calculated density profiles for different types of atoms along the bilayer normal. The extent of the bilayer is clearly delineated by the peaks of the lipid head group nitrogen and phosphorus atoms (Figure 3). The profiles further show that water molecules penetrate the entire length of the channel pore for both the nAChR and GlyR. These results were consistent over four independent simulation runs including (i) the entire nAChR, (ii) the nAChR TM domain with an initially water-filled pore, (iii) the nAChR TM domain with an initially empty pore, and (iv) the GlyR TM domain with an initially empty pore. Thus, the outcome was independent of whether the pore was water-filled in the initial model. From Figure 3c, it is evident that for the nAChR, water density is minimal at the center of the pore (z coordinate between -2.5 and 2.5 Å) corresponding to the hydrophobic girdle formed by Val 13′. Indeed, visual inspection of the trajectories shows that water in the constriction zone can on occasion be reduced to chains of just three or four individual water molecules. The GlyR pore, by contrast, is substantially more polar, lined with serine and threonine residues (Figure 2), and thus is more hydrated at the center than the pore of nAChR. The extracellular end of the GlyR pore (z coordinate above 2 Å) is especially well-hydrated, whereas the intracellular end shows a somewhat reduced water density. The narrowest section of the GlyR pore corresponded to a group of threonine residues at position 6′ along the M2 helix (z coordinate 10 Å; Supporting Information Figure S1).

Adaptive biasing force calculations[15] were used to examine the proposal that the gate is a hydrophobic obstruction and to assess the contribution of the pore to ion selectivity in both the nAChR and GlyR. The resulting one-dimensional potentials of mean force (PMFs) for all four possible cases of receptor, cation, and anion are presented in Figure 4.

The PMF for sodium inside the nAChR pore features two distinct areas of ion stabilization toward the extracellular end, corresponding to two distinct sets of negatively charged residues, D27′ and E20′. In both positions a sodium ion is stabilized by ∼2 kcal/mol. Multiple ions can be accommodated at position D27′ due to the large pore radius at that position of the lumen. Thus, the two extracellular rings of negatively charged residues serve as a funnel for cations, increasing their local concentrations. Snapshots from the trajectories showing these interactions are presented in Figure 5, panels a and b. Below position 17′, the pore narrows substantially to a radius of ∼2.5 Å (Supporting Information Figure S1). In this region the M2 helices expose primarily hydrophobic residues toward the interior of the receptor (Leu9′, Val13′, Phe14′, and Leu16′). The PMF in this region undergoes a steep increase and reaches an overall maximum at $z \sim 0$ Å, in good correspondence with the region of maximum hydrophobicity identified in the water density profile (Figure 3c). This result is in agreement with ideas regarding the hydrophobic nature of the gate based on the cryo-EM structure of nAChR.[4] The height of the barrier is approximately 5 kcal/mol relative to the minimum of the PMF at $z \sim -10$ Å and can be attributed both to the change in the local electrostatics (Figure 6) and partial desolvation of the ion (Supporting Information Figure S2). The effective free energy of sodium in the entire intracellular region of the pore (z between 0 and 20 Å) remains largely unfavorable compared to bulk solvent and goes through several minor peaks and troughs. For instance, the minima at -9 and -18 Å correspond to polar residues—serine 10′ for the first minimum and threonine 6′ and serine 2′ for the second. Interestingly, the PMF indicates a

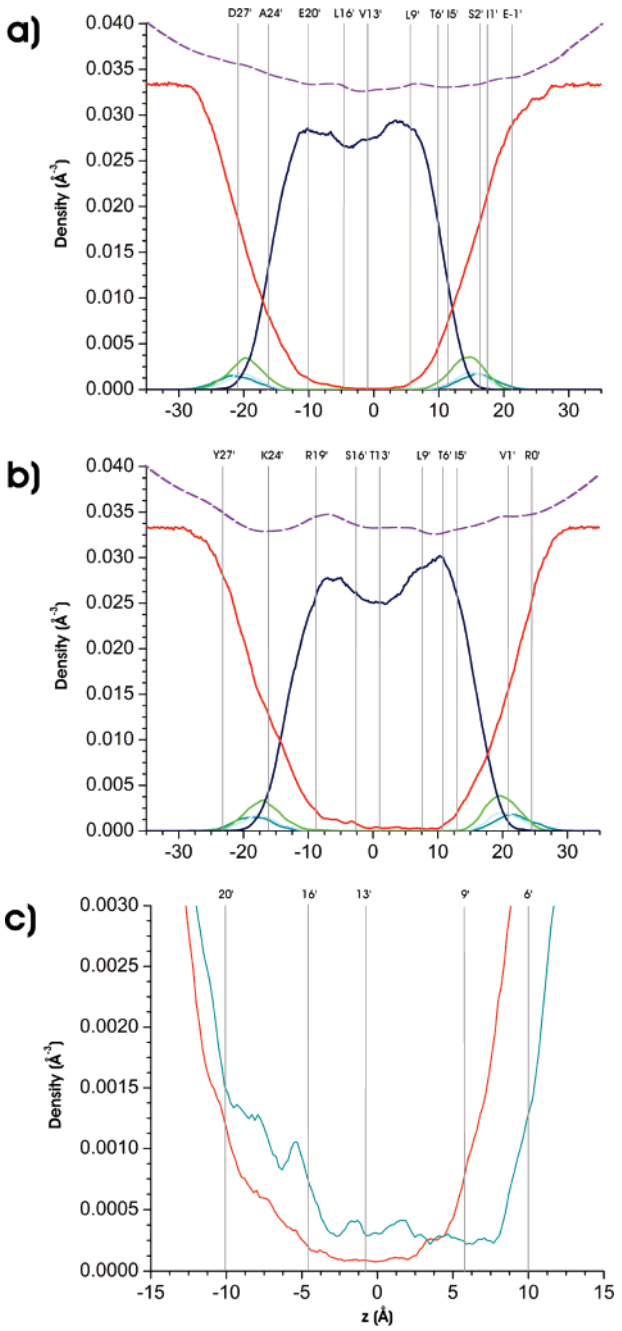

Figure 3. Density profiles along the lipid bilayer normal for lipid tail carbon (dark blue), lipid head group nitrogen (light blue), phosphorus (dark cyan), and ester oxygen atoms (green) as well as water oxygen atoms (red) for (a) nAChR and (b) GlyR. (c) Amplified version of the density profiles for water oxygen atoms in GlyR (cyan) and nAChR (red). Positions of M2 pore-lining residues are shown with gray lines and labeled at the top of the graphs. Average pore radius profiles along the channel axis obtained using the program HOLE are shown by a dashed line (purple) for nAChR in panel a and GlyR in panel b, respectively. The scale for the pore radius in not shown; refer to Supporting Information Figure S1 for details.

(14) Anishkin, A.; Sukharev, S. *Biophys. J.* **2004**, *86*, 2883−2895.
(15) Chipot, C.; Henin, J. *J. Chem. Phys.* **2005**, *123*, 244906.

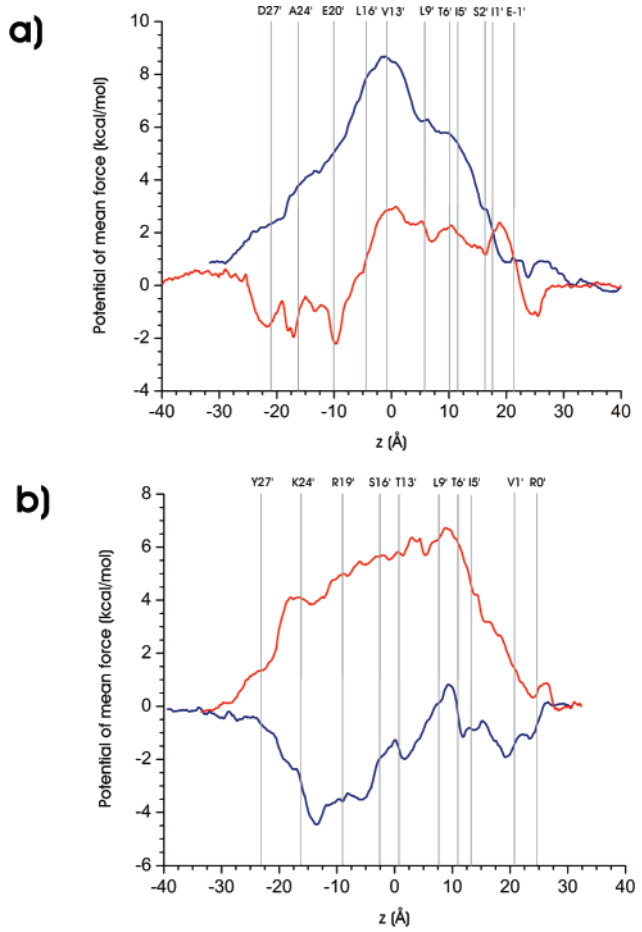

Figure 4. Potentials of mean force for translocation of Na^+ ions (red) and Cl^- ions (blue) in (a) nAChR and (b) GlyR. Positions of the M2 pore-lining residues are shown with gray lines and labeled at the top of the graphs.

barrier for sodium at the very exit of the channel ($z \sim -20$ Å) on the intracellular side, associated primarily with Ile 1′. Its height is comparable to the overall maximum in the free energy profile at the center of the TM domain. Inspection of the trajectory for that window in the PMF profile shows that the sodium ion possesses an intact first solvation shell. However, the second solvation shell can be severely disrupted by the side chains of isoleucine residues. A corresponding barrier is missing in the GlyR due to its larger pore radius at the intracellular end. The sharp decline in the sodium PMF for the nAChR at $z \sim -25$ Å is due to specific interactions of the ion with an oppositely charged girdle of glutamate residues at position −1′ upon exiting the pore.

The PMF for chloride inside the nAChR pore is clearly distinct from the one for sodium, displaying no region of appreciable stabilization anywhere inside the TM domain and a broad maximum toward the middle of the pore that is likely due to both unfavorable electrostatics and hydrophobicity. The overall barrier in the PMF for chloride is on the order of 8 kcal/mol, leading to a channel effectively closed to anions. While the position of the overall barrier agrees very well with the corresponding hydrophobic region in the sodium PMF, the profiles are quite different at the intracellular end, indicating that a Cl^- ion can enter the vestibule without significant disruption of its solvation shell and can be better stabilized by serine and threonine residues than can a solvated Na^+ ion.

The effective free energy profile for a chloride ion in the TM domain of GlyR receptor (Figure 4b) reveals, perhaps unexpectedly, no hydrophobic barrier in the middle of the pore. In stark contrast to the nAChR case, the only barrier observed in the PMF corresponds to the ring of leucine residues in position 9′, which would seem to be easily surmountable by thermal fluctuations. The exact magnitude of the barrier is subject to relatively small statistical error (less than 0.5 kcal/mol) from ABF sampling. However, we note the potential uncertainties associated with homology modeling of GlyR based on the structure of *Torpedo* nAChR as well as deficiencies in the force field. We also note that polarizability effects (not explicitly accounted for in our simulations) may be important in modeling chloride ions as opposed to the smaller and less polarizable sodium ions. Nevertheless, there is compelling evidence that ion translocation through GlyR proceeds, qualitatively, through a substantially smaller barrier as compared to nAChR. In retrospect, this finding can be attributed to the fact that two of the three hydrophobic pore-lining residues in the nAChR have been replaced by polar residues (threonine and serine) in the GlyR, with L9′ being the only exception (Figure 2). Furthermore, in the GlyR the L9′ side chains face away from the center of the pore and pack against the hydrophobic side chains from the neighboring M1 helix. Coupled with the significant hydration of the pore at the 9′ position, this orientation allows for passage of chloride ions without substantial disruption from hydrophobic interactions. Thus, our results do not appear to substantiate a purely hydrophobic gate in the middle of the GlyR pore and may indicate additional structural contributions to the gate in the GlyR as compared to nAChR.

We also found significant stabilization at the extracellular end of the GlyR by residues from positions 24′ through 19′ of the M2 helix. The observed stabilization appears largely due to electrostatic interactions of the chloride ion with a ring of K24′ residues (shown in Figure 5d)). The lysine side chains extend inward toward the center of the pore where they very effectively stabilize the anion. By contrast the Arg residues at position 19′ do not provide specific stabilization to anions but rather influence the local electrostatic potential at the center of the pore. The Arg side chains orient away from the pore in the model structure and, therefore, do not directly contact chloride ions inside the extracellular vestibule.

The free energy profile for a sodium ion in the TM domain of GlyR receptor (Figure 4b) displays largely unfavorable interactions for the ion throughout the length of the TM domain. The overall barrier to permeation is ∼7 kcal/mol—analogous to the reverse case of chloride translocation through the nAChR receptor. The position of the PMF maximum is also located at the narrowest section of the pore, which for the GlyR receptor occurs at $z \sim 10$ Å. A snapshot of the trajectory of a chloride ion in this region of the pore, associated with positions 9′ and 6′, is shown in Figure 5f.

The PMF profiles suggest that the electrostatics of the pore contribute substantially to charge selectivity. In both receptors the PMF profiles display low free energy wells on the extracellular side of M2, corresponding to the extracellular rings of charge, which would be expected to concentrate the permeating ions and repel the oppositely charged ions. Appropriately charged residues at the intracellular end of the TM domains of both receptors (E-1′ for nAChR; R0′ for GlyR) form intracellular

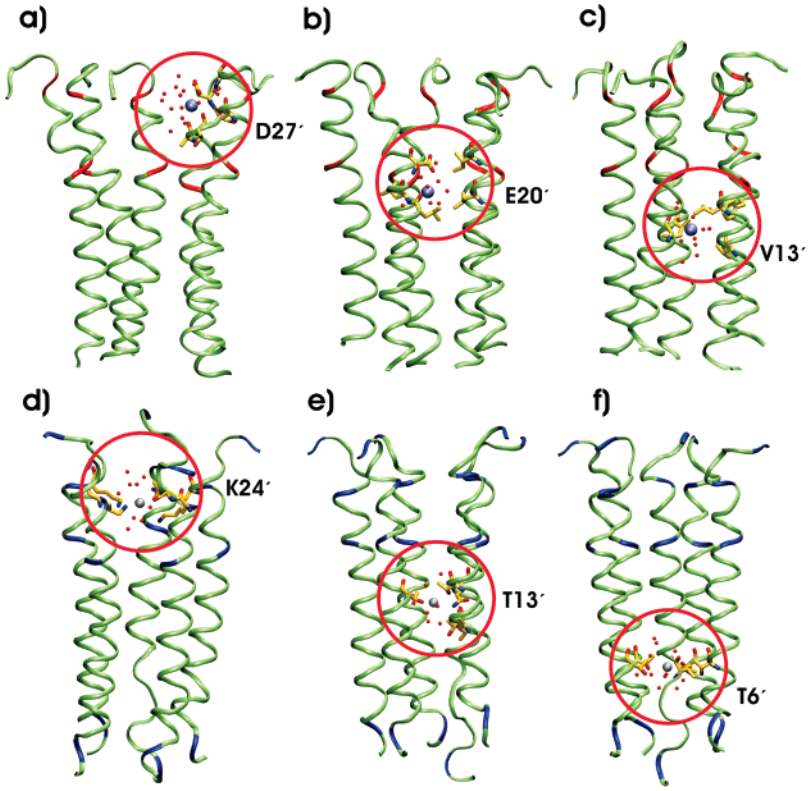

Figure 5. Trajectory snapshots depicting the translocation of a Na^+ ion (purple) at different positions along the pore of nAChR with the closest pore-lining residues labeled (panels a−c). Trajectory snapshots depicting the translocation of a Cl^- ion (gray) at different positions along the pore of GlyR with the closest pore-lining residues labeled (panels d−f).

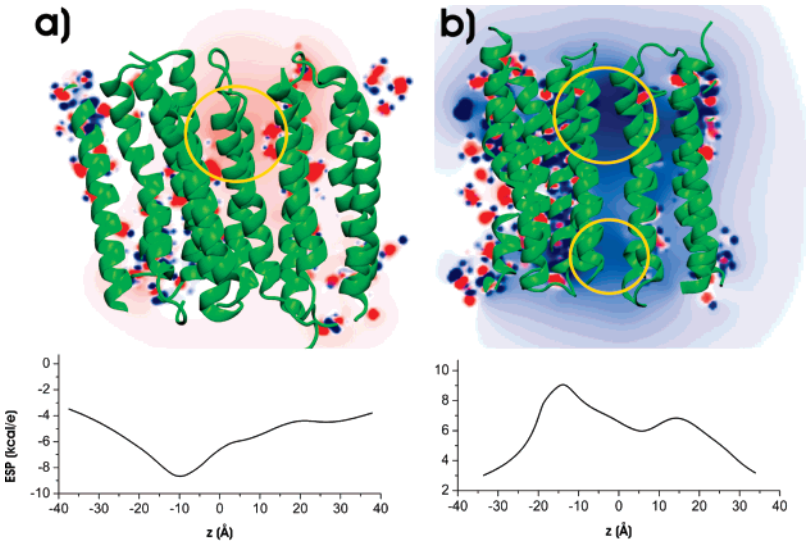

Figure 6. Electrostatic potential (ESP) profiles along the channel pore from APBS calculations for (a) nAChR and (b) GlyR. The positive potential is shown in blue, the negative potential is in red; the peaks in the two profiles are indicated with yellow circles.

rings of charge, which would also seem to stabilize the permeating ion.

Our models for GlyR and nAChR are based on the structure of *Torpedo* nAChR obtained without a ligand and, therefore, presumably reflect the resting closed state of the channel. Structural changes inferred from cryo-EM of the *Torpedo* receptor with and without bound ACh suggested a rotation of the five M2 helices, causing collapse of a central hydrophobic girdle.[16] However, subsequent studies have yielded a mixed picture. A simple dilation mechanism was suggested by assessment of residues that line the pore in the open state using proton block of the channel after lysine substitution,[17] while placement of Zn^{2+} binding sites at various levels in the pore suggested a tilting of the M2 helices.[7] In the absence of high-resolution structural information on the open state of the receptor it is necessary to comment on the robustness of our conclusions regarding selectivity. Our results suggest that selectivity in nAChR is largely determined by multiple rings of charged

(16) Unwin, N. *Nature* **1995**, *373*, 37−43.

(17) Cymes, G. D.; Ni, Y.; Grosman, C. *Nature* **2005**, *438*, 975−980.

residues positioned at the entrance and exit of the channel pore that favor or disfavor the passage of ions based on charge. Such a "nonspecific" mechanism to discriminate between ions of different charge would be insensitive to moderate perturbations affecting the pore in the open state since ion recognition would not require precise tuning of the selectivity filter as is the case, notably, for the potassium channels. Tilting of M2 or dilation the pore in the open channel does not result in a structure dramatically different from that of the closed channel. Rotation in the open state would only impact our results if the conformational change in M2 was so pronounced as to expose a completely different set of residue side chains toward the center of the pore.

Finally, the presence of a hydrophobic restriction in the lower segment of the pore-lining M2 helices for α7 nAChR corroborates the notion of hydrophobic gating in nAChR. It also suggests that the features of the channel responsible for gating and for selectivity are distinct. If the location of the gate is distinct from the location of the selectivity filter subtle changes in the orientation of the M2 helices leading to an open pore would have no effect on the observed preference for cations versus anions.

To gain deeper insight into the electrostatic contributions to ion selectivity, we used Poisson−Boltzmann electrostatics calculations. The resulting electrostatic potential (ESP) profiles reveal deep potential wells for the permeating ion in the extracellular halves of each receptor pore (Figure 6). Thus, the ESP profiles confirm an electrostatic mechanism for concentrating permeating ions and repelling oppositely charged ions, thus assisting ion flow toward the intracellular end. This contribution is further confirmed by the ESP profile generated after switching the charge of the residue at position 20′ of the nAChR, which shows a highly destabilizing potential peak at the same position as that of the stabilizing well in the nonmutant (Supporting Information Figure S3). This result predicts a decrease in the conductance of the permeating cation, which agrees with mutagenesis experiments showing substantial changes in conductance after mutating this ring of charged residues.[18,19] Experimentally, the E20′ position has been implicated in channel rectification, and consecutive mutations from E to A at position 20′ led to a progressive reduction in conductance.[18,20,21] Analogous results have been obtained from mutational experiments on the ring of K24′ residues in the GlyR receptor, which parallel our findings with respect to inversion of the local ESP upon charge-altering mutations.

We note that a recent study by Beckstein and Sansom determined the PMF for sodium and chloride ion translocation through the M2 helix bundle of the *Torpedo* nAChR and found essentially no stabilization of Na^+ at positions equivalent to 20′.[22] We attribute the difference to the fact that the *Torpedo* structure has only three negatively charged (E) and two neutral (A) residues in that region of the pore. The glutamate residues are further engaged in salt bridges, which provide a much more charge-balanced environment than in the case of the homopentameric α7 nAChR. We also note the high salt concentration (1 M) used in the Beckstein and Sansom study, which may have resulted in better screening of the glutamate residues by counterions.

The ESP profiles further reveal that, in contrast to the extracellular rings of charges, the intracellular rings contribute differently to the local electrostatics of the pore in the two receptors. In the nAChR there is little electrostatic stabilization, whereas in the GlyR there is a second stabilizing potential well. This could be attributed to differences in the side chain orientations of residues in position −1′/0′ away from the pore in the two receptors. Also, the K0′ residue in the nAChR may provide sufficient screening to negate the local electrostatic effect of the neighboring −1′ glutamates.

It should be pointed out that definitive assessment of the electrostatic contribution in the region of the intracellular ring (positions −2′ to 2′) is not possible due to the relatively low resolution of 4 Å in the cryo-EM structure and potential artifacts from homology modeling. Triple mutation at positions −1′ (E/A), −2′ (insertion P), and 13′ (V/T) has been shown to reverse ionic selectivity in α7 nAChR,[23] α1 GlyR,[24] and 5HT3 receptors,[25] highlighting the contribution of the intracellular end of the M2 helix to selectivity. However, ESP profiles for the triple mutant in the α7 nAChR show little change from the nonmutant (Supporting Information Figure S3). It should be noted that the low resolution of the structure in that region, and the fact that the N-terminus is essentially unconstrained due to truncation of the preceding protein chain, precludes definitive assessment of the orientations for these specific residues.

Concluding remarks

Computationally demanding adaptive biasing force simulations were carried out to investigate structural mechanisms of ion translocation and selectivity in the α1 GlyR and α7 nAChR ligand-gated ion channels. Our calculations provide new insights into the dynamic and energetic mechanisms of ion permeation that complement the growing body of experimental mutational and structural data for these receptors. The barriers for translocation of oppositely charged ions were found to be different in both receptors. Thus, selectivity could be partially attributed to rings of charged residues at the extracellular and intracellular ends of the receptor pore and to the overall electrostatics of the TM domain. The extracellular rings served as a funnel for ions, increasing the concentration of oppositely charged ions at the entrance and exit of the pore. Indeed, the extracellular end of the nicotinic receptor was wide, fully hydrated, and appeared to accommodate multiple sodium ions through interactions with two rings of negatively charged residues. Similarly the glycine receptor was able to stabilize multiple chloride ions at the extracellular mouth of the channel. Water density profiles showed that for both nAChR and GlyR the channel pore was completely water-filled. Although water could freely permeate the entire length of the channel pore, the same was not true for solvated ions. Indeed, the sodium PMF for nAChR revealed a hydrophobic restriction with a maximum barrier at positions

(18) Imoto, K.; Busch, C.; Sakmann, B.; Mishina, M.; Konno, T.; Nakai, J.; Bujo, H.; Mori, Y.; Fukuda, K.; Numa, S. *Nature* **1988**, *335*, 645−648.
(19) Kienker, P.; Tomaselli, G.; Jurman, M.; Yellen, G. *Biophys. J.* **1994**, *66*, 325−334.
(20) Keramidas, A.; Moorhouse, A. J.; Schofield, P. R.; Barry, P. H. *Prog. Biophys. Mol. Biol.* **2004**, *86*, 161−204.
(21) Rajendra, S.; Lynch, J. W.; Pierce, K. D.; French, C. R.; Barry, P. H.; Schofield, P. R. *Neuron* **1995**, *14*, 169−175.
(22) Beckstein, O.; Sansom, M. S. *Phys. Biol.* **2006**, *3*, 147−159.
(23) Corringer, P. J.; Bertrand, S.; Galzi, J. L.; Devillers-Thiery, A.; Changeux, J. P.; Bertrand, D. *Neuron* **1999**, *22*, 831−843.
(24) Keramidas, A.; Moorhouse, A. J.; French, C. R.; Schofield, P. R.; Barry, P. H. *Biophys. J.* **2000**, *79*, 247−259.
(25) Gunthorpe, M. J.; Lummis, S. C. *J. Biol. Chem.* **2001**, *276*, 10977−10983.

9′−13′ leading to a pore closed to ions. This finding is in agreement with ideas about the hydrophobic nature of the gate in nAChR. By contrast, the PMFs for GlyR revealed no significant barriers to ion translocation arising from hydrophobic effects. Our simulations reproduce many key aspects of the channels' ion selectivity and together with recently improved structural knowledge can serve as a basis for further inquiry into the mechanism of ion permeation in the ligand-gated ion channel family.

Materials and Methods

Homology Models. Homology models of the homopentameric human α7 nAChR receptor and the α1 GlyR were constructed using the program Modeller 8.[26] The models were based on the 4.0 Å resolution cryo-EM structure of nAChR from *T. marmorata* (PDB accession code: 2BG9).[3] Only the TM domain was considered in the modeling procedure. No symmetry was imposed on the five identical subunits of the receptors.

Simulation Details. The homology models of the TM domain of nAChR and GlyR were embedded in a fully hydrated, palmitoyl-2-oleoyl-*sn*-glycerol-phosphatidylcholine (POPC) bilayer patch of dimensions 120 Å × 120 Å (containing 297 individual lipids for the nAChR model and 290 lipids for the GlyR model). The models were completed by adding hydrogen atoms and solvated with 21860 TIP3P[27] water molecules for nAChR and 21185 water molecules for GlyR. Charge neutralization was accomplished with the addition of Na^+ and Cl^- ions. Excess salt concentration (∼0.1 M) was introduced in order to mimic physiological conditions.

The system underwent 2000 steps of initial energy minimization to remove unfavorable contacts followed by 50 000 steps of constant volume molecular dynamics. The temperature was gradually increased from 50 to 310 K during this period. Harmonic restraints (with force constant of 3 kcal·mol^{-1}·Å^{-2}) were imposed on the protein Cα atoms. These restraints were scaled down in four stages and eventually removed in the course of an extensive 2 ns equilibration in the constant surface area ensemble.

The production runs were also performed in the constant surface area ensemble with the program NAMD2.6[28] and the CHARMM27 force field.[29] A short-range cutoff of 9 Å was used for nonbonded interactions, and long-range electrostatic interactions were treated with a particle mesh Ewald method.[30] Langevin dynamics and a Langevin piston algorithm were used to maintain the temperature at 310 K and a pressure of 1 atm. The r-RESPA multiple time step method[31] was employed with a 2 fs time step for bonded interactions, 2 fs for short-range nonbonded interactions, and 4 fs for long-range electrostatic interactions. The bonds between hydrogen and heavy atoms were constrained with the SHAKE algorithm.[32]

All simulations were carried out on the DataStar machine at the San Diego Supercomputer Center. The density profiles in Figure 3 were calculated by binning the *z*-coordinate positions of the atoms for each species (lipid tail carbon, lipid head group nitrogen, phosphorus, ester oxygen atoms, and water oxygen atoms) to construct a histogram. The bin size was 0.2 Å, and density was normalized by the volume of a 0.2 Å wide slab of the simulation box oriented perpendicular to the bilayer normal. The program VMD was used in the visualization and analysis of the results.[33]

Adaptive Biasing Force Method. The adaptive biasing force method as implemented in the NAMD2.6 package by Chipot and Henin[15] was used to determine the effective free energy profiles discussed above. The method couples ideas from thermodynamic integration and average force formalisms with unconstrained molecular dynamics and the introduction of an adaptive biasing potential. Briefly, a predefined intuitive coordinate ξ has to be selected. The average force experienced by the simulated system at any point along this coordinate is estimated from the instantaneous forces experienced by the system at that position. The average forces are accumulated in bins along ξ and are continuously updated as the simulation progresses. The estimated free energy derivative, computed for small intervals of ξ, is canceled by the introduction of an adaptive biasing potential. The application of the adaptive bias allows the system to overcome existing barriers along ξ in the free energy landscape.

In our case the translocation coordinate (z) was chosen as the normal to the bilayer surface. The simulations were carried out in 10 windows of length 5 Å along this direction and were sufficient to cover the entire length of the TM domain region of the two receptors. Additional windows of ∼7−8 Å length were used to extend the PMFs to the region of bulk solvent on both sides of the channel pore. For these extra windows a cylindrical confining potential was applied in order to prevent the ion from drifting too far from the axis of the pore in the plane parallel to the bilayer.[34] Within each window the average force acting on the selected ion was accumulated in 0.1 Å sized bins. Smoothing within 0.2 Å was applied by averaging the content of adjacent bins. Since the instantaneous forces acting on the ion can fluctuate considerably, it is desirable to delay the application the adaptive bias until adequate number of force samples has been collected. Therefore, application of the adaptive bias was initiated only after the accumulation of 800 samples in individual bins. Subsequently, the biasing force was introduced progressively in the form of a linear ramp. Harmonic restraints (with force constant of 3 kcal·mol^{-1}·Å^{-2}) were applied to six Cα carbon atoms on each subunit (three at the M2−M3 linker at the extracellular end and three at the M1−M2 linker at the intracellular end of the TM domain). It should be emphasized that these restraints are not coupled to the reaction coordinate through common atoms so that the corresponding forces have no direct influence upon the PMF calculation. Production runs in each window were continued for at least 3 ns, resulting in a total simulation time of more than 150 ns.

Electrostatic Potential Calculations. Poisson−Boltzmann electrostatics calculations were carried out using the APBS package.[35] The charge and radius parameters for APBS were assigned by using PDB2PQR server.[36] CHARMM force field charges were used.[29] The detailed set of APBS parameters included (i) protein dielectric of 2.0, (ii) solvent dielectric of 78.54, (iii) solvent radius 1.4 Å, (iv) temperature of 298.15 K, (v) ionic salt concentration 0. M, (vi) grid dimensions of 193 × 193 × 193, and (vii) grid spacing ∼ 0.5 Å.

Acknowledgment. This research was funded by NSF and NIH. Additional support was provided by the NSF Center for Theoretical Biological Physics, National Biomedical Computational Resource, and Accelrys, Inc. I.I acknowledges support from the Burroughs Wellcome Fund/La Jolla Interfaces in Science fellowship. Computer resources were provided by the Pittsburgh Supercomputing Center and the San Diego Supercomputer Center.

(26) Sali, A.; Blundell, T. L. *J. Mol. Biol.* **1993**, *234*, 779−815.
(27) Jorgensen, W. L.; Chandrasekhar, J.; Madura, J. D.; Impey, R. W.; Klein, M. L. *J. Chem. Phys.* **1983**, *79*, 926−935.
(28) Phillips, J. C.; Braun, R.; Wang, W.; Gumbart, J.; Tajkhorshid, E.; Villa, E.; Chipot, C.; Skeel, R. D.; Kale, L.; Schulten, K. *J. Comput. Chem.* **2005**, *26*, 1781−1802.
(29) MacKerrell, A. D.; Bashford, D.; Bellott, M.; Dunbrack, R. L.; Evanseck, J. D.; Field, M. J.; Fischer, S.; Gao, J.; Guo, H.; Ha, S.; et al. *J. Phys. Chem. B* **1998**, *102*, 3586−3616.
(30) Darden, T.; York, D.; Pedersen, L. *J. Chem. Phys.* **1993**, *98*, 10089−10092.
(31) Tuckerman, M.; Berne, B. J.; Martyna, G. J. *J. Chem. Phys.* **1992**, *97*, 1990−2001.
(32) Ryckaert, J. P.; Ciccotti, G.; Berendsen, H. J. C. *J. Comput. Phys.* **1977**, *23*, 327−341.
(33) Humphrey, W.; Dalke, A.; Schulten, K. *J. Mol. Graphics Modell.* **1996**, *14*, 33−38.
(34) Allen, T. W.; Andersen, O. S.; Roux, B. *Proc. Natl. Acad. Sci. U.S.A.* **2004**, *101*, 117−122.
(35) Baker, N. A.; Sept, D.; Joseph, S.; Holst, M. J.; McCammon, J. A. *Proc. Natl. Acad. Sci. U.S.A.* **2001**, *98*, 10037−10041.
(36) Dolinsky, T. J.; Nielsen, J. E.; McCammon, J. A.; Baker, N. A. *Nucleic Acids Res.* **2004**, *32*, 665−667.

Supporting Information Available: Average pore radius profiles, a plot of the average number of water molecules in the first solvation shell of sodium inside the nAChR pore, electrostatic potential profiles for a set of mutations in the sequence of the M2 helices, and coordinates for the nAChR and GlyR models (in PDB format). This material is available free of charge via the Internet at http://pubs.acs.org.

JA070778L